Renewable Energy 161 (2020) 1359–1367

Contents lists available at ScienceDirect

Renewable Energy

journal homepage: www.elsevier.com/locate/renene

Investigation of aerodynamic performance characteristics of a wind-turbine-blade profile using the finite-volume method

Onur Erkan [a], Musa Özkan [a, *], T. Hikmet Karakoç [b], Stephen J. Garrett [c], Peter J. Thomas [d]

[a] Department of Mechanical Engineering, Bilecik Şeyh Edebali University, Bilecik, TR-11230, Turkey
[b] Faculty of Aeronautics and Astronautics, Eskişehir Technical University, Eskişehir, TR-26470, Turkey
[c] School of Mathematics and Actuarial Science, University of Leicester, Leicester, LE1 7RH, UK
[d] Fluid Dynamics Research Centre, School of Engineering, University of Warwick, Coventry, CV4 7AL, UK

ARTICLE INFO

Article history:
Received 30 September 2019
Received in revised form
27 March 2020
Accepted 28 July 2020
Available online 8 August 2020

Keywords:
Aerodynamic performance
Blade profile
Finite volume method
Numerical simulation
Wind turbines

ABSTRACT

Two-dimensional incompressible flow around a NACA 63–415 airfoil, which is encountered in engineering applications as a typical wind-turbine-blade profile, is investigated computationally. Aerodynamic loads and the flow mechanism over this particular blade profile are examined in detail to determine the optimum angle of attack. Simulations are performed in the range of the typical operating conditions encountered for commercial-scale wind turbines with Reynolds numbers $10^5 \leq Re \leq 3 \times 10^6$ and for angles of attack $0^\circ \leq \alpha \leq 20^\circ$. The turbulent flow was modelled by means of the Spalart-Allmaras and the Shear-Stress Transport (SST) k-ω turbulence models to provide a direct comparison between data obtained with different models. The results obtained are compared to numerical and experimental data available in literature for validation. The aerodynamic performance analysis reveals that the optimum angle of attack for this blade profile is $\alpha = 6^\circ$ for $Re \leq 10^6$ and $\alpha = 7^\circ$ for $Re \geq 1.6 \times 10^6$.

1. Introduction

The global usage of renewable energy, as an alternative to conventional energy resources, has reached approximately 10.4% of the total energy production and continues to increase [1]. Wind energy, specifically, is one of the most important renewable resources since it is accessible in most parts of the world and since it constitutes a continuous and reliable energy source to drive wind turbines.

Although wind energy can provide almost steady and dependable power, using this energy effectively can be difficult. The very first constraint regarding the generation of electricity using wind turbines is the Betz coefficient. This is known as Betz's law which indicates the limitations of a wind turbine as regards extracting a fraction of the available total kinetic energy of the wind [2]. According to this law, the efficiency of wind turbines is restricted to approximately 59.3%. In addition to this limit, unavoidable factors such as surface roughness due to contamination, erosion and icing, as well as design parameters (e.g. the angle of attack) have a significant effect on the aerodynamic efficiency of wind turbine blade profiles. Due to the large number of the relevant parameters, investigations on wind-turbine efficiency remain to be a challenging and vibrant research topic [3].

The angle of attack, α, of the wind turbine blade (cf. Fig. 1) as a design parameter is one of the most crucial aspects in the industrial wind-turbine design and it has been intensively studied for many different profiles of turbine blades [5–9]. The current investigation focusses on the determination of the lift to drag ratio of the blade. This represents the ratio of the acting lift and drag force, indicated in Fig. 1, on the blade geometry. Following Liu et al. [10], the lift force and the drag force are given by, respectively, Equation (1) and Equation (2).

$$F_L = \frac{1}{2} \times \rho \times C_L \times A_L \times V^2 \tag{1}$$

$$F_D = \frac{1}{2} \times \rho \times C_D \times A_D \times V^2 \tag{2}$$

here, ρ is the density of air, A_L is the projected wing area, A_D is the rotor blade's cross-sectional area and V is the velocity of the oncoming air. The quantities C_L and C_D are referred to, respectively, as the lift and the drag coefficients. The lift to drag ratio is defined as C_L/C_D and is mostly used as an indicator of efficiency [9,11–13].

* Corresponding author.
E-mail address: musa.ozkan@bilecik.edu.tr (M. Özkan).

https://doi.org/10.1016/j.renene.2020.07.138
0960-1481/

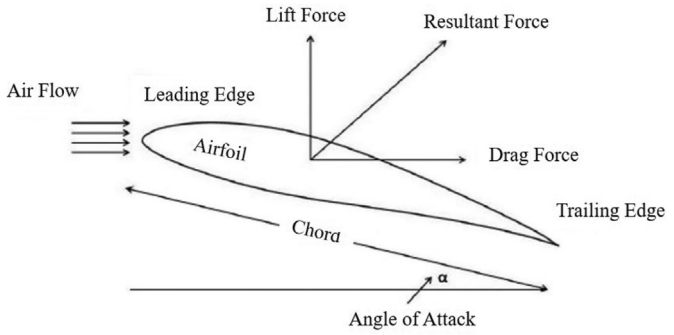

Fig. 1. Forces acting on an airfoil [4].

Note that Equations (1) and (2) are not predictive. Knowledge of C_L and C_D is required to find F_L and F_D but the two coefficients remain unknown unless experiments or computational simulations have been performed for the particular airfoil under consideration.

The US National Advisory Committee for Aeronautics (NACA) has developed numerous different airfoil shapes. These are referred to by the prefix NACA followed by a series of digits identifying the characteristics of the particular airfoil (cf. Section 2.1). The NACA 63−415 airfoil is one of the most commonly used blade profiles for commercial wind turbines [14]. For instance, a wind turbine with a power capacity of 1.8 MW, produced by the manufacturer Vestas Wind Systems A/S, is composed of a NACA 63 XXX blade profile between the blade tip and its centre [15]. However, the determination of the optimum angle of attack for this specific airfoil has been rarely studied in the literature.

Chaudhary and Nayak [12], for instance, examined the flow over the NACA 63−415 profile using only the Shear-Stress Transport (SST) $k-\omega$ turbulence model and within limited ranges of the angle of attack and the Reynolds number, for the purpose of comparison with data for a NACA 63−412 airfoil. They concluded that the NACA 63−415 airfoil performs better as a wind turbine blade than NACA 63−412 for the particular flow conditions investigated in that study. The results of Chaudhary and Nayak [12] motivated the current study to investigate the optimum angle of attack for the NACA 63−415 airfoil for a broader range of flow conditions and, in particular, by also implementing different turbulence models. In the current study, the analyses were, therefore, performed in the range of $Re = 10^5 \leq Re \leq 3 \times 10^6$ and angles of attack $0^\circ \leq \alpha \leq 20^\circ$. The Reynolds number used in this study is given by Equation (3) where c is the chord length and μ is the dynamic viscosity of air.

$$Re = \frac{\rho V c}{\mu}. \tag{3}$$

Moreover, Vendan et al. [16] investigated the flow over the NACA 63−415 profile for low Reynolds numbers by means of solely the Spalart-Allmaras turbulence model. They reported that the optimum angle of attack under their low Reynolds number flow conditions is $\alpha = 2^\circ$. However, the optimum angle of attack needs to be considered not only for low Reynolds numbers but also for the parameter regime that covers the operating conditions of a commercial-scale wind turbine.

The shortcomings of the studies by Chaudhary and Nayak [12] and Vendan et al. [16] motivated the current research to analyze the flow over the NACA 63−415 airfoil as a wind turbine blade over a wider range of the Reynolds numbers and for various angles of attack. Here incompressible, two-dimensional (2D) flow over the NACA 63−415 airfoil is examined computationally by means of the commercial Computational Fluid Dynamics (CFD) software, Fluent, and by using the Reynolds-Averaged Navier Stokes (RANS) based Spalart-Allmaras [17] and SST $k-\omega$ [18] schemes to model turbulence. The Spalart-Allmaras turbulence model is a well-known approach to model aerodynamic flows [19–21]. Similarly, the SST k-ω model is widely used for the investigation of flow over NACA airfoils [22–24]. Suvanjumrat [25], for instance, compared different turbulence models and concluded that the SST k-ω model is suitable for the simulations of flow over NACA airfoils. Furthermore, it has been shown that the SST k-ω model can provide precise results for flows with an adverse pressure gradient [23] and flows over airfoils where flow separation of the boundary layer occurs [26,27].

Moreover, the application of CFD for the investigations of the flow mechanism around turbine blades is quite common since it can provide valuable insights into rotor aerodynamics which is a principal factor for maximizing the efficiency of transforming wind energy into mechanical energy [22]. Currently, commercial wind-turbine blade-design procedures are based on Blade Element Momentum (BEM) theory [28]. Nevertheless, numerical studies concerning the aerodynamic performance of a rotor can range from BEM models integrated by CFD simulations to full three-dimensional (3D) Navier-Stokes solutions. Prior to the comprehensive design of the wind turbine power production, investigations of the rotor aerodynamics by means of 2D CFD approaches can represent valuable contributions to the research area of wind energy. Furthermore, as it is stated by Ge et al. [24], 3D secondary flows, such as the spanwise flow, are often less important for a rotor blade section far away from the hub and the tip since the flow here is governed by the streamwise flow.

Sayed et al. [9], for instance, investigated the flow over blade profiles S809 and S826 at low Reynolds numbers by means of 2D numerical finite-volume simulations. Successively, Sayed et al. [22] performed 2D aerodynamic examinations for different blade profiles at high wind speeds. Moreover, NACA 0008 and NACA 0012 blade profiles were aerodynamically analysed by Hoogedoorn et al. [29] at high Reynolds numbers ($Re > 10^6$) using 2D CFD-RANS simulations. Mohamed [30], additionally, performed 2D numerical investigations for 20 different airfoils including NACA 00XX and NACA 63XXX series for comparison. Two-dimensional CFD simulations were also compared with experimental results by Singh et al. [31] and a good agreement was observed in pressure distribution over their blade profile. Another comparison with experimental results were carried out by Daróczy et al. [32] for the flow over H-Darrieus rotor blades. Experimental data were compared with 2D CFD results obtained by various turbulence models and eventually, the Realizable k-ε and the SST k-ω models were reported as best prediction models in 2D numerical examinations. Wang et al. [33] compared their 2D numerical results of power coefficients for the airfoil shapes investigated with the experimental data of Castelli et al. [34] and stated that there is a reasonable agreement between their results even though the tip losses are ignored in 2D modelling.

Consequently, the current study will initially proceed to compare and validate the different turbulence models to establish that they represent suitable means for investigating flows around NACA airfoils. In the main part of the study, the optimum angle of attack for the NACA 63−415 airfoil is determined for a wide parameter range covering the typical operation conditions of wind turbines. The results of this research benefit the design process of new commercial wind-turbine blades, modifying existing ones and it can serve as a benchmark simulation study in the area of the applications of CFD to practical engineering problems.

2. Material and method

The characteristics of the airfoil considered in this study are

summarized. Thereafter the governing equations and the numerical scheme employed for the research are introduced.

2.1. The airfoil

Airfoils from the NACA family have been widely used as blades for commercial wind turbines since experimental data for most of these profile types are readily available in the literature and through NACA [35–37]. The NACA 63–415 profile was used in the current research due to the lack of comprehensive examination of the flow over this particular airfoil type [14]. Furthermore, the NACA 63–415 airfoil has been shown to display good stall characteristics such that it is often used for stall-regulated wind turbines [38].

Each digit following the NACA series prefix in the name of the airfoil quantifies a characteristic of the airfoil [35,36,38,39]:

- The first digit states the series of the airfoil {6}.
- The second digit identifies the distance of the minimum pressure area in tens of percent of chord {3}.
- The third digit specifies the lift coefficient in tenths {4}.
- The last two digits indicate the maximum thickness as percent of chord {15}.

2.2. Governing equations

A steady-state, two-dimensional, incompressible flow over the rotor blade profile is considered. The flow is governed by the steady-state Reynolds-Averaged Navier-Stokes (RANS) equations, describing momentum conservation, together with requirement for mass conservation. The two relevant expressions are given by, respectively, Eqs. (4) and (5) [26,40,41].

$$\frac{\partial}{\partial x_j}(\rho u_i u_j) = -\frac{\partial p}{\partial x_i} + \frac{\partial}{\partial x_j}\left[\mu\left(\frac{\partial u_i}{\partial x_j} + \frac{\partial u_j}{\partial x_i} - \frac{2}{3}\delta_{ij}\frac{\partial u_l}{\partial x_l}\right)\right] + \frac{\partial}{\partial x_j}\left(-\rho\overline{u_i' u_j'}\right) \tag{4}$$

$$\frac{\partial}{\partial x_i}(\rho u_i) = 0 \tag{5}$$

In these two expressions ρ is the average density, p is the average pressure, μ is the dynamic viscosity and $(-\rho\overline{u_i' u_j'})$ is the Reynolds stresses. For a proper turbulence modelling, in the Reynolds-averaged method, the Reynolds stresses need to be suitably modeled. A common approach adopted employs the Boussinesq hypothesis [42] relating the Reynolds stresses to the mean velocity gradients as shown in Equation (6).

$$-\rho\overline{u_i' u_j'} = \mu_t\left(\frac{\partial u_i}{\partial x_j} + \frac{\partial u_j}{\partial x_i}\right) - \frac{2}{3}\left(\rho k + \mu_t\frac{\partial u_i}{\partial x_i}\right)\delta_{ij} \tag{6}$$

To close the RANS equations, that is to obtain a sufficient number of equations for all unknowns of the problem, the turbulent (eddy) viscosity μ_t and the turbulent kinetic energy k need to be described by means of additional transport equations that depend on the particular turbulence model used.

2.3. The CFD model

The geometry considered in the CFD simulations is shown in Fig. 2, it was defined by means of coordinate data acquired from the NACA airfoil tools web site [37].

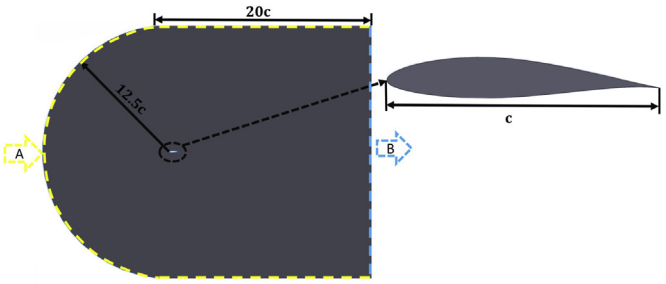

Fig. 2. The CFD model and boundary conditions.

The discretization of the CFD model employs the C-type structured mesh shown in Fig. 3. This mesh structure is known to minimize the calculation time for the type of CFD problems considered here [43,44]. The proper discretization of the computational domain is crucial since there may be boundary layer separation over the blade profile at higher angles of attack and, moreover, because von Kármán vortices can be formed downstream of the airfoil. Accordingly, a careful mesh independence test was conducted and the details of this test are discussed in Section 3.1.

Velocity inlet and pressure outlet boundary conditions were assigned to regions A and B in Fig. 2, respectively. The pressure outlet was defined as atmospheric pressure and velocities at the inlet were calculated for associated the Reynolds numbers of $Re = 10^5$, $Re = 5\times10^5$, $Re = 7\times10^5$, $Re = 10^6$, $Re = 1.6\times10^6$, and $Re = 3\times10^6$. Different angles of attack, in the range of $0^\circ \le \alpha \le 20^\circ$, were set by means of the components of the inlet velocity. The main geometric parameters of the tested airfoil and the computational domain together with the boundary conditions are listed in Table 1 where c represents the chord length of the airfoil.

The surface of the blade profile was defined as a smooth wall and a no-slip boundary condition was applied at this surface. Values $\rho = 1.1614 kg/m^3$ for the density of air and $\mu = 1.846\times10^{-5} kg/ms$ for the dynamic viscosity were used. The convergence criterion was chosen as 10^{-10} for all flow simulations involving both the Spalart-Allmaras and the SST $k-\omega$ turbulence model.

Despite the fact that the Spalart-Allmaras turbulence model was also used for comparison, the main outcome of this research was obtained by means of the SST $k-\omega$ turbulence model since it is proven to be the best option for the predictions of rotor aerodynamics [23,32,33,45–47]. SIMPLE algorithm for pressure-velocity coupling was employed to solve the RANS equations and the convection terms were discretized with second-order upwind

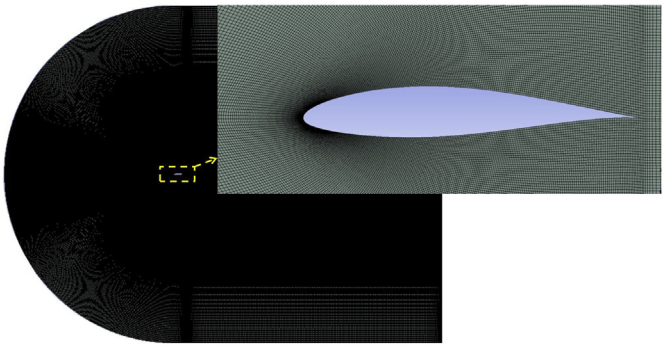

Fig. 3. The discretization of the CFD model using C-type structured mesh.

Table 1
The main geometric parameters of the tested airfoil and the computational domain together with the boundary conditions (c is the chord length).

Airfoil Features		Computational Domain		Boundary Conditions	
AirfoilCategory	NACA 6-Series	RectangleWidth	20c	Section A	VelocityInlet
AirfoilName	NACA63–415	Radius	12.5c	Section B	PressureOutlet
Max. ThicknessValue	0.15c			AirfoilSurface	SmoothWall
Max. ThicknessPosition	0.35c				
Max. CamberValue	0.022c				
Max. CamberPosition	0.5c				

scheme. Following Ge et al. [24], the transition from laminar to turbulent flow was simulated by means of the $\gamma - Re_\theta$ transition model.

3. Results and discussion

3.1. Mesh independence test

As indicated in Section 2.3 the importance of the mesh structure for this particular problem results from the high possibility of the occurrence of the boundary layer separation on the blade surface and the formation of eddies downstream of the blade. These flow phenomena usually cause stability issues and, thus, convergence problems. Therefore, a thorough mesh independence test was conducted as a part of this study.

Simulations were initially conducted using coarse mesh structures with 16,950 mesh elements. The number of mesh elements was then increased in successive steps to investigate the effects on the overall results of the simulations. The lift coefficient C_L and the drag coefficient C_D of the blade profile were used as control parameters for each mesh configuration and the results are shown in Fig. 4. The data displayed in the figure reveal that the lift coefficient and the drag coefficient remain nearly constant, at $C_L \cong 0.8$ and $C_D \cong 0.012$, for the number of mesh elements 218,163 and above. Therefore, the number of mesh elements used in this research was chosen as 322,806 to ensure stable solutions and convergence.

The mesh structure determined by the independence test provided a value for the nondimensional wall distance in the range of $1 \leq y^+ \leq 5$ which is appropriate for the investigations of boundary layer flows [48,49].

The wall y^+ value is given by Equation (7) where τ_w is the wall-shear stress, ρ is the density of air, y is the distance of the centre of the first cell to the nearest wall and ν is the kinematic viscosity of air. In addition to the first mesh element near the wall that provides the range of $1 \leq y^+ \leq 5$, there are 20 grid points in the viscous sublayer to secure the solution of high velocity and pressure gradients in the vicinity of walls.

$$y^+ = \frac{\sqrt{\tau_w/\rho} \times y}{\nu}. \tag{7}$$

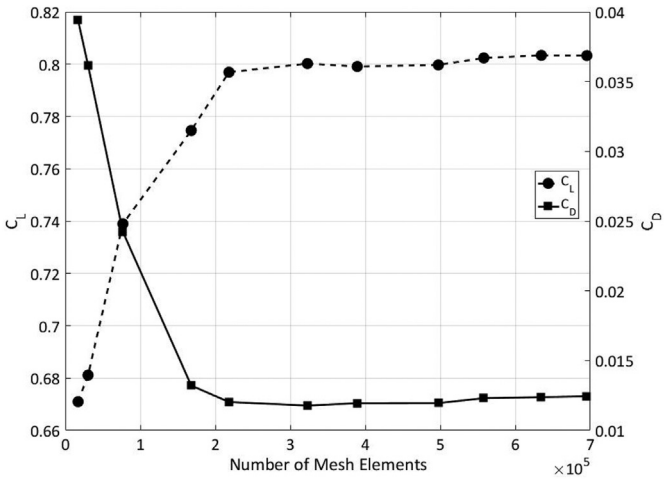

Fig. 4. The results of the mesh independence test at $Re = 10^5$ and $\alpha = 5^\circ$.

3.2. Validation of the numerical model

The lift coefficient was acquired for twenty different angles of attack in the range of $0^\circ \leq \alpha \leq 20^\circ$ and by means of both turbulence models. These results were then compared with the available numerical and experimental data in literature.

Fig. 5 displays experimental data obtained by Abbott and von Doenhoff [35] at $Re = 3 \times 10^6$ in comparison to associated computational results of the current study. The figure reveals an overall good agreement between the experimental data and the simulations based on the two different turbulence models used. In particular, Fig. 5 shows that, for higher angles of attack ($\alpha \geq 13^\circ$), the SST $k-\omega$ turbulence model predicts the lift coefficient better than the Spalart-Allmaras turbulence model.

Fig. 6 shows computational results of the current study in

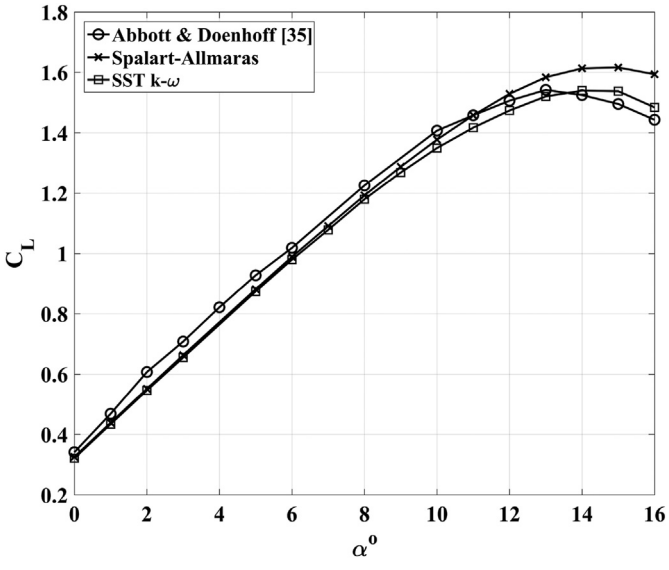

Fig. 5. Comparison between computational C_L results of the current study and the experimental data of Abbott and von Doenhoff [35] for $Re = 3 \times 10^6$.

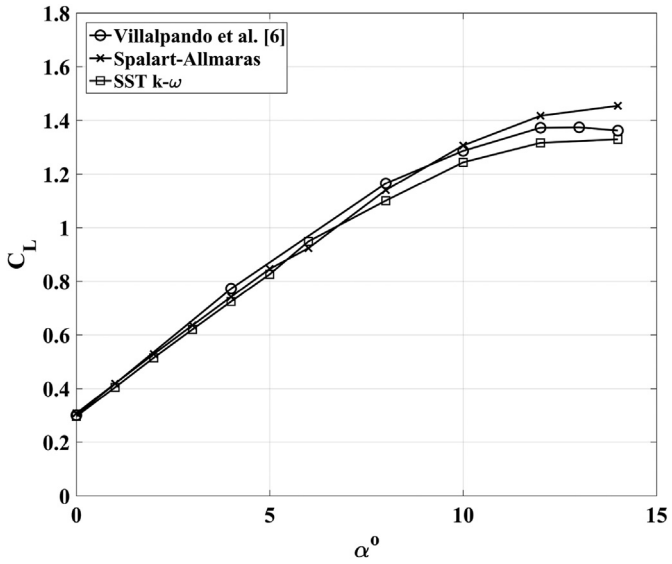

Fig. 6. Comparison between the computational C_L data of the current study and the numerical data of Villalpando et al. [6] for $Re = 5 \times 10^5$.

comparison to numerical data reported by Villalpando et al. [6] for $Re = 5 \times 10^5$. It is clear from the figure that, especially in the range of $0^\circ \leq \alpha \leq 7^\circ$, there is a very close agreement between the current numerical results and the computational data provided by Villalpando et al. [6]. For $\alpha \geq 7^\circ$, the agreement still continues with insignificant discrepancies.

The computational drag coefficient data of the current study produced by the SST k-ω turbulence model is also compared with the experimental data of Bak et al. [50] in Fig. 7. Bak et al. [50] conducted their 2D wind tunnel experiments of a NACA 63−415 airfoil for $Re = 1.6 \times 10^6$ with minimizing the 3D effects by means of end plates. They reported that the stall characteristics of this commonly used airfoil as a wind turbine blade profile can be improved by using a modified profile introduced by Fuglsang and Bak [51]. This comparison shows a very good agreement between the present numerical data and the experimental results for approximately $\alpha \leq 12^\circ$. Above this angle of attack, there is a strong possibility of a flow separation but the CFD model can still reasonably predict the experimental data.

The capability of the current numerical models for predicting the drag coefficient is also verified by means of the comparison with the computational data of Villalpando et al. [6] which is displayed in Fig. 8. As previously stated for Fig. 7, two numerical models of the current study completely agree in Fig. 8. The predictions of the current study also agree very well with the results of Villalpando et al. [6] up to approximately $\alpha \leq 10^\circ$. Above this angle of attack very minor discrepancies are observed. Additionally, the SST $k-\omega$ model seems to better produce the data of Villalpando et al. [6] in the range of $10^\circ \leq \alpha \leq 15^\circ$.

The data in Figs. 5–8 have shown that the computational results of the current study employing the SST $k-\omega$ model agree more favourably with both computational and experimental data from the literature than our data obtained by means of the Spalart-Allmaras model. For the investigation of the optimum angle of attack in the remainder we will, therefore, proceed by employing the SST $k-\omega$ model only.

3.3. Optimum angle of attack

The optimum angle of attack for the NACA 63−415 airfoil, using the SST k-ω turbulence model, was determined for twenty different angles of attack, equally spaced between $0^\circ \leq \alpha \leq 20^\circ$, at each of the six Reynolds numbers of $Re = 10^5$, $Re = 5 \times 10^5$, $Re = 7 \times 10^5$, $Re = 10^6$, $Re = 1.6 \times 10^6$ and $Re = 3 \times 10^6$.

Fig. 9 displays the variation of the lift coefficient C_L as a function of the angle of attack, α, for the six different Reynolds numbers investigated. The figure shows that the lift coefficient increases with the angle of attack up to $\alpha \approx 12^\circ$. For larger angles of α, there are slight changes in the tendencies of the plots for each of the six Reynolds numbers investigated. Subsequently, the lift coefficient drops at $\alpha \gtrsim 15^\circ$. This is a well-known, general phenomenon known as stall for such flows over blade profiles. The phenomenon occurs for sufficiently large angles of α when the boundary layer is no longer able to stay attached to the surface of the body and separates from it. This boundary-layer separation is associated with a sudden decrease in the lift force. The flow separation at $\alpha = 15^\circ$ and for $Re = 7 \times 10^5$ can be clearly seen in Fig. 10. Fig. 9 reveals, moreover, that the lift coefficient, characterizing to the lift force, is obviously

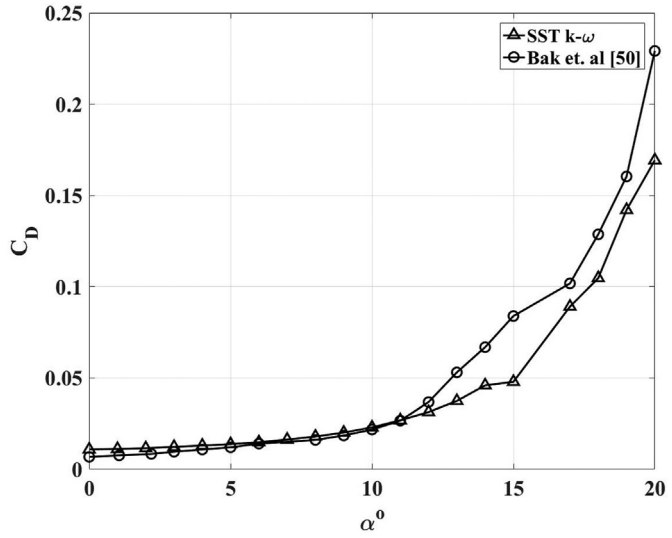

Fig. 7. Comparison between the computational C_D data of the current study and the experimental data of Bak et al. [50] for $Re = 1.6 \times 10^6$.

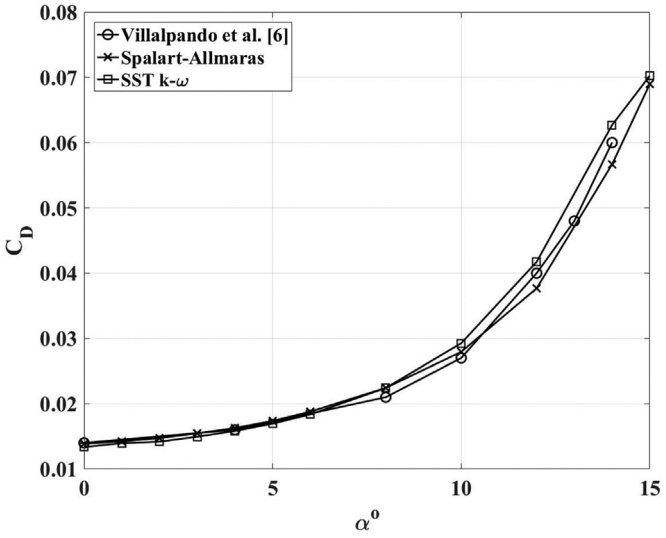

Fig. 8. Comparison between the computational C_D data of the current study and those of Villalpando et al. [6] for $Re = 5 \times 10^5$.

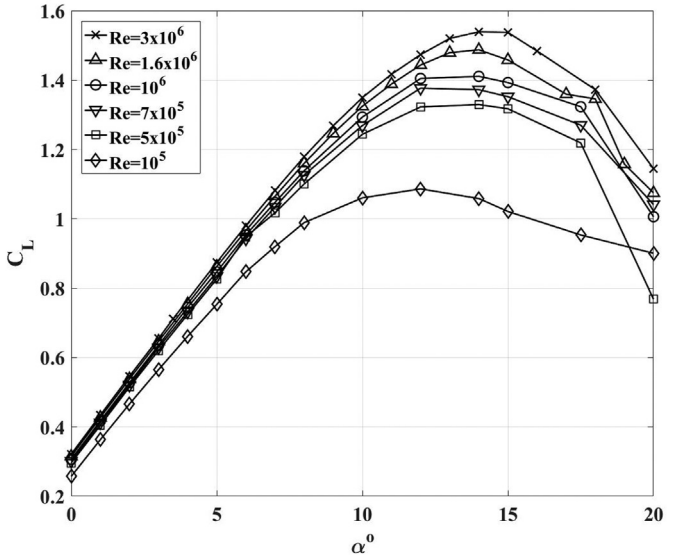

Fig. 9. The change in the lift coefficient C_L as a function of the angle of attack α for the six different Reynolds numbers investigated.

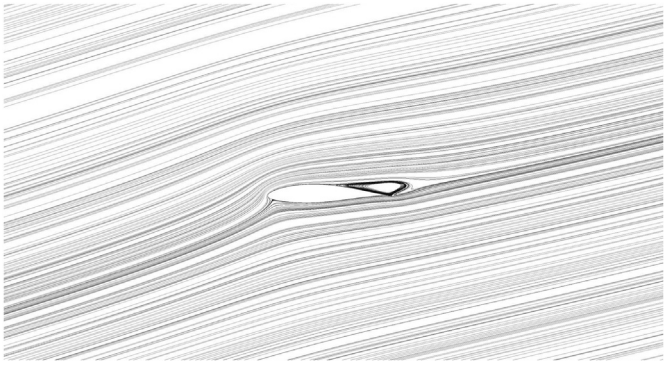

Fig. 10. Flow separation over the blade profile for $\alpha = 15^\circ$ and $Re = 7 \times 10^5$.

larger for higher Reynolds numbers.

The values of the drag coefficient C_D for different angles of attack α and for the six Reynolds numbers investigated are illustrated in Fig. 11. The range of the drag coefficient displayed by this figure is in the range $0 \leq C_D \leq 0.3$, this agrees with data reported by several other studies for such airfoils [12,52]. Similar to the lift coefficient, the drag coefficient increases with the angle of attack. However, unlike in the case of the lift coefficient, there is no sudden decrease in the drag coefficient after a specific value of the angle of attack.

Additionally, Fig. 11 reveals that for smaller α, the drag coefficient only increases weakly with the angle of attack. However, for $\alpha \gtrsim 12^\circ$, this increase is exponential. This is also expected since for low angles of attack the drag force mainly arises from viscous effects (skin friction) but at higher angles of attack, boundary layer separation occurs and form drag effects are included which then constitute the dominant factor.

Furthermore, the drag coefficient decreases with increasing Reynolds number. This is due to the fact that a turbulent boundary layer occurs with an increase in Reynolds number. By this means the flow remains attached to the surface and the boundary layer separation does not occur. Therefore, the drag force is reduced with an increase in Reynolds number.

It is difficult to determine the optimum angle of attack by considering the lift and drag coefficients separately because as the

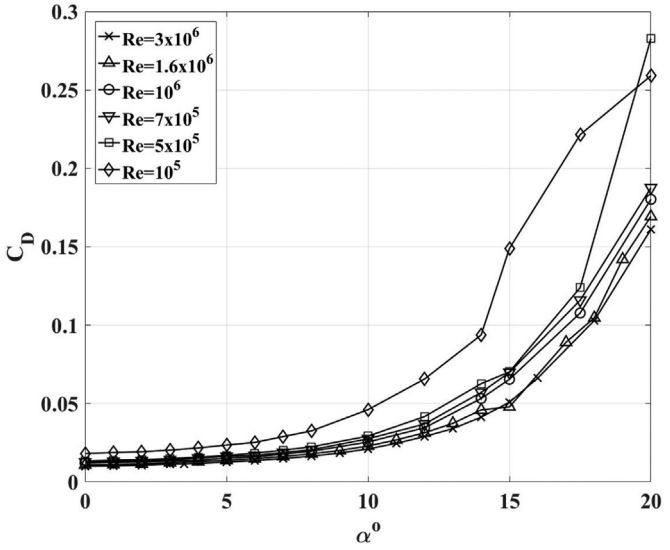

Fig. 11. The change in the drag coefficient C_D as a function of the angle of attack α for the six different Reynolds number values investigated.

lift coefficient is raised, the lift force acting on the blade profile that powers the turbine is increased. However, an increase in the drag force is also observed which is not desired as it reduces the output power produced by the wind turbine. Therefore, the lift to drag ratio C_L/C_D is considered as an indicator of efficiency.

The change of the lift to drag ratio is shown in Fig. 12. The maximum value of this ratio should indicate the optimum angle of attack for the blade profile investigated. Thus, it can be seen from the figure that for every Reynolds number, the maximum of C_L/C_D occurs somewhere between 5° and 8°. For determining a specific value for the optimum angle of attack, maxima of C_L/C_D ratio at each value of Reynolds number investigated are plotted in Fig. 13. From this figure it can be concluded that the optimum angle of attack is $\alpha = 6^\circ$ for the Reynolds number of $Re \leq 10^6$ and $\alpha = 7^\circ$ for $Re \geq 1.6 \times 10^6$.

Previously, optimum angles of attack of $\alpha = 2^\circ$ [12] and

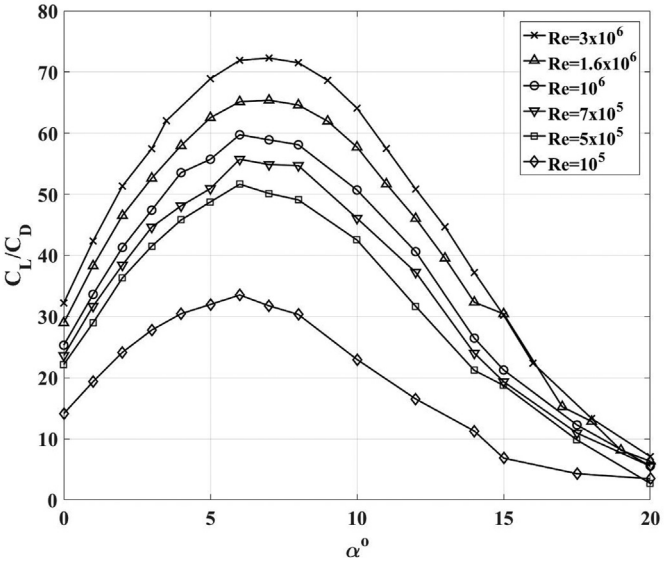

Fig. 12. The lift to drag ratio C_L/C_D as a function of the angle of attack α for simulations employing the SST k-ω turbulence model.

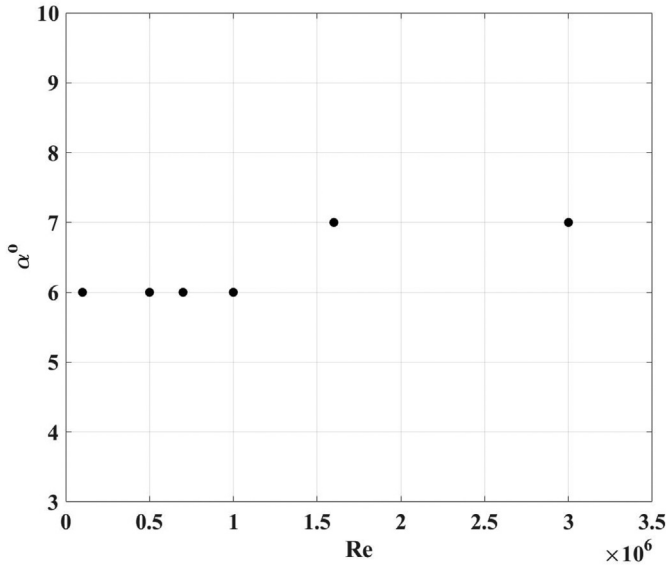

Fig. 13. The optimum angle of attack α at each value of Reynolds number investigated.

$\alpha = 5.25^\circ$ [16] were found. Moreover, Yilmaz et al. [52] reported values of the optimum angle of attack in the very broad range of 4° to 12°. The current study, nevertheless, precisely provides the optimum angle of attack as $\alpha = 6^\circ$ or 7° depending on the Reynolds number for the NACA 63–415 type blade profile by means of a turbulence model whose reliability is proven in literature by many different studies.

To further examine the effects of the acquired optimum angle of attack on rotor aerodynamics, the distribution of the surface pressure coefficient C_p is shown in Fig. 14 for $\alpha = 0^\circ$ and in Fig. 15 for $\alpha = 8^\circ$. The distribution of C_p for $\alpha = 8^\circ$ instead of the optimum angle of attack is provided since Bak et al. [50] only reported values for $\alpha = 8^\circ$ which is very close to the optimum value nevertheless. It can be seen from these figures that the current numerical results are entirely consistent with the experimental data.

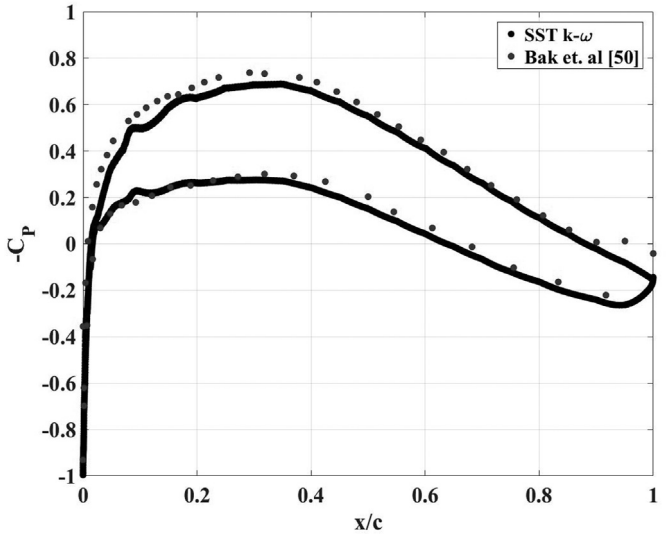

Fig. 14. Distribution of the surface pressure coefficient C_p for the NACA 63–415 airfoil at $Re = 1.6 \times 10^6$ and $\alpha = 0^\circ$. Black dotes indicate current computational data and blue dots indicate the experimental data of Bak et al. [50]. (For interpretation of the references to colour in this figure legend, the reader is referred to the Web version of this article.)

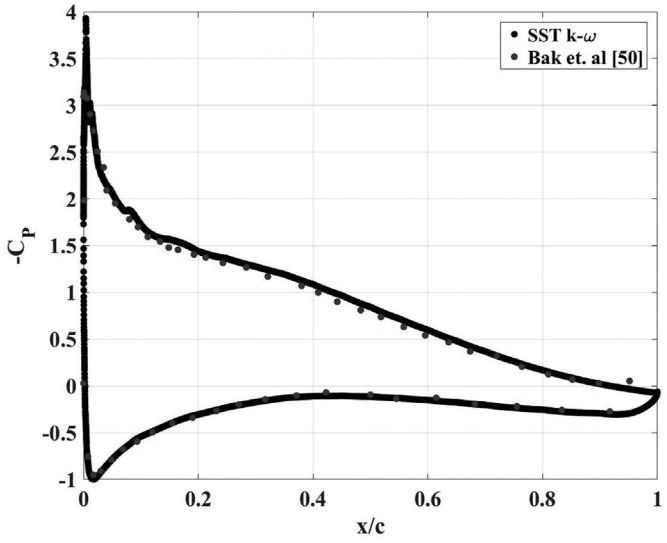

Fig. 15. Distribution of the surface pressure coefficient C_p for the NACA 63–415 airfoil at $Re = 1.6 \times 10^6$ and $\alpha = 8^\circ$. Black dotes indicate current computational data and blue dots indicate the experimental data of Bak et al. [50]. (For interpretation of the references to colour in this figure legend, the reader is referred to the Web version of this article.)

Moreover, the differential pressure between the pressure side and the suction side is not dissimilar at the trailing edge of the airfoil for both angles of attack. However, the difference in pressure between the pressure and the suction side at the leading edge is increased with the application of the angle of attack $\alpha = 8^\circ$. Consequently, transforming wind energy into mechanical energy is more effective with the attack angle of $\alpha = 8^\circ$ that is close to the optimum values found as $\alpha = 6^\circ$ and 7°.

Moreover, Figs. 16 and 17 show the pressure contours for the NACA 63–415 blade profile at $\alpha = 0^\circ$ and $\alpha = 6^\circ$, respectively. The pressure distributions are obtained for the wind speed that is corresponding to $Re = 7 \times 10^5$. In both figures, the pressure is lower at suction side than the pressure side as a result of the increase in the velocity above the airfoil. This pressure difference, as stated in Figs. 14 and 15, causes the lift force that rotates the wind turbine. Furthermore, the pressure above the blade profile raises from the leading edge to the trailing edge. Due to the fact that the pressure is higher at the trailing edge than the leading edge, the adverse pressure gradient is encountered which is related to the boundary-

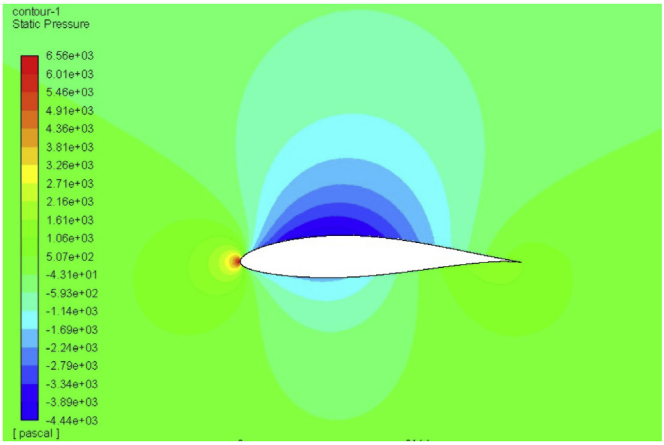

Fig. 16. Pressure contours for the NACA 63–415 profile at $\alpha = 0^\circ$ and $Re = 7 \times 10^5$.

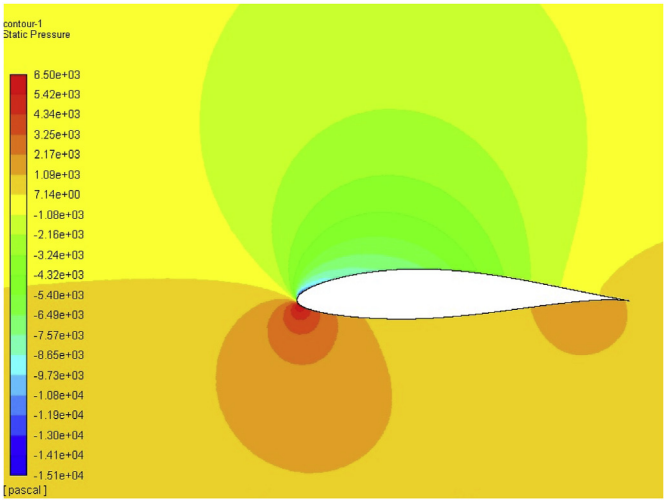

Fig. 17. Pressure contours for the NACA 63–415 profile at $\alpha = 6^\circ$ and $Re = 7 \times 10^5$.

layer transition and perhaps the separation, if this gradient is excessively strong. The comparison between pressure contours, which is another example of insights into flow mechanisms, displays that with the use of the optimum angle of attack, the blade profile becomes aerodynamically more effective.

4. Conclusion

The efficiency of a wind turbine depends on many aspects such as the characteristics of the wind, which cannot be controlled, and the surface roughness of the blades resulting from contamination, erosion, icing and etc. Obviously, the design parameters of the blades also have crucial effects on the effectiveness. The angle of attack is the most critical design parameter for turbine blades and therefore its influence on the efficiency needs to be studied by means of investigating the flow over these airfoils.

Hence, in this study, a two-dimensional, steady-state, incompressible flow over a NACA 63–415 airfoil, which is widely used as blades of commercial wind turbines, was examined numerically by means of CFD model introduced in preceding sections.

Simulations were carried out in the range of Reynolds number between $Re = 10^5 \leq Re \leq 3 \times 10^6$ and for the angles of attack $0^\circ \leq \alpha \leq 20^\circ$. These two parameter ranges cover the most commonly encountered operating conditions for commercial-scale wind turbines.

The Spalart-Allmaras and the SST k-ω turbulence models were used to simulate turbulent flow. This enabled a direct comparison between results obtained by two different turbulence models and also provided data for comparison with literature data. An in-depth mesh independence test was performed followed by the validation of the CFD model.

The data obtained revealed that the SST k-ω turbulence model produces results which compare more favourably to computational and experimental literature data than the Spalart-Allmaras turbulence model. The SST k-ω model was employed to determine the range for the optimum angle of attack.

The lift coefficient and the drag coefficient, which characterize the lift force and the drag force acting on the airfoil, were examined for various angles of attack at different Reynolds numbers. Both coefficients increase with an increase in the angle of attack. However, there is a critical range of the angle of attack, $12^\circ - 15^\circ$, after which a decrease in the lift coefficient observed.

Separate investigations of these two coefficients revealed no clear information regarding the performance of the blade and thus the wind turbine. Therefore, the lift to drag ratio is considered as an indicator of the effectiveness of the blade. The observation of the maxima of this ratio for various angles of attack shows that the optimum angle of attack is $\alpha = 6^\circ$ for the Reynolds number of $Re \leq 10^6$ and $\alpha = 7^\circ$ for $Re \geq 1.6 \times 10^6$. The turbine blade is considered to have the highest aerodynamic performance at these values.

In addition to the angle of attack as a design parameter, the surface roughness of the blade can be implemented in the subsequent studies to investigate the flow and to see whether that parameter influence the optimum angle of attack for the NACA 63–415 airfoil since the surface roughness is mostly an unavoidable aspect for wind turbine blades.

CRediT authorship contribution statement

Onur Erkan: Methodology, Formal analysis, Investigation, Writing - review & editing. **Musa Özkan:** Conceptualization, Methodology, Writing - original draft, Writing - review & editing, Supervision. **T. Hikmet Karakoç:** Writing - review & editing, Supervision. **Stephen J. Garrett:** Writing - review & editing, Supervision. **Peter J. Thomas:** Writing - review & editing, Supervision, Project administration.

Declaration of competing interest

The authors declare that they have no known competing financial interests or personal relationships that could have appeared to influence the work reported in this paper.

Acknowledgements

This research did not receive any specific grant from funding agencies in the public, commercial, or not-for-profit sectors.

Appendix A. Supplementary data

Supplementary data to this article can be found online at https://doi.org/10.1016/j.renene.2020.07.138.

References

[1] Renewable Energy Policy Network for the 21st Century, Renewables 2018 Global Status Report, 2018. Tech. rep., Paris, France.
[2] A. Betz, Introduction to the Theory of Flow Machines, Pergamon Press, Oxford, UK, 1966.
[3] A. Varol, C. İlkılıç, Y. Varol, Increasing the efficiency of wind turbines, J. Wind Eng. Ind. Aerod. 89 (9) (2001) 809–815, https://doi.org/10.1016/S0167-6105(01)00069-1.
[4] P. Durga Charan, M. Devi Prasad, CFD simulations for the selection of an appropriate blade profile for improving energy efficiency in axial flow mine ventilation fans, J. Sustain. Min. 13 (1) (2014) 15–21, https://doi.org/10.7424/jsm140104.
[5] C. Thumthae, T. Chitsomboon, Optimal angle of attack for untwisted blade wind turbine, Renew. Energy 34 (5) (2009) 1279–1284, https://doi.org/10.1016/j.renene.2008.09.017.
[6] F. Villalpando, M. Reggio, A. Ilinca, Numerical study of flow around iced wind turbine airfoil, Eng. Appl. Comput. Fluid Mech. 6 (1) (2012) 39–45, https://doi.org/10.1080/19942060.2012.11015401.
[7] I. Şahin, A. Acir, Numerical and experimental investigations of lift and drag performances of NACA 0015 wind turbine airfoil, Int. J. Mach. Mach. Mater. 3 (2015) 22–25, https://doi.org/10.7763/IJMMM.2015.V3.159.
[8] M.M.M. Saad, S.B. Mohd, M.F. Zulkafli, W.M.E. Shibani, Numerical analysis for comparison of aerodynamic characteristics of six airfoils, AIP Conf. Proc. 1831 (1) (2017), 020004, https://doi.org/10.1063/1.4981145.
[9] M.A. Sayed, H.A. Kandil, E.S.I. Morgan, Computational fluid dynamics study of wind turbine blade profiles at low Reynolds numbers for various angles of attack, AIP Conf. Proc. 1440 (1) (2012) 467–479, https://doi.org/10.1063/1.4704251.
[10] M. Liu, L. Tan, S. Cao, Cavitation-vortex-turbulence interaction and one-dimensional model prediction of pressure for hydrofoil ALE15 by Large Eddy Simulation, J. Fluid Eng. 141 (2) (2018), 021103, https://doi.org/10.1115/

1.4040502.
[11] W. Chakroun, I. Al-Mesri, S. Al-Fahad, Effect of surface roughness on the aerodynamic characteristics of a symmetrical airfoil, Wind Eng. 28 (5) (2004) 547–564, https://doi.org/10.1260/0309524043028136.
[12] U. Chaudhary, S.K. Nayak, Micro and small-scale HAWT blades airfoils study through CFD for low wind applications, in: 2015 Annual IEEE India Conference, INDICON, 2015, pp. 1–6, https://doi.org/10.1109/INDICON.2015.7443703.
[13] M.N. Mohd Hafiz, A.H. Ahmad Hussein, R. Helmi, W. Wirachman, S.N. Mohd, Wind tunnel experiment for low wind speed wind turbine blade, in: Mechanical and Aerospace Engineering, ICMAE2011, vol. 110, Trans Tech Publications Ltd, 2012, pp. 1589–1593, https://doi.org/10.4028/www.scientific.net/AMM.110-116.1589, of Applied Mechanics and Materials.
[14] C. Hochart, G. Fortin, J. Perron, A. Ilinca, Wind turbine performance under icing conditions, Wind Energy 11 (4) (2008) 319–333, https://doi.org/10.1002/we.258.
[15] Anonymous, V80-1.8MW Pitch Regulated Wind Turbine with OptiSlip and OptiTip, Tech. rep., Vestas Wind Systems A/S, Denmark, 2004.
[16] S. Vendan, S. Aravind Lovelin, M. Manibharathi, C. Rajkumar, Analysis of a wind turbine blade profile for tapping wind power at the regions of low wind speed, Int. J. Mech. Eng. 2 (2) (2010) 1–10.
[17] S. Spalart, S. Allmaras, A One-Equation Turbulence Model for Aerodynamic Flows, Tech. Rep. Technical Report AIAA-92-0439, American Institute of Aeronautics and Astronautics, 1992.
[18] F.R. Menter, Two-equation eddy-viscosity turbulence models for engineering applications, AIAA J. 32 (8) (1994) 1598–1605, https://doi.org/10.2514/3.12149.
[19] S. Azmahani, N.A.M. Yunus, A.H. Saiful Anuar, A.E. Ismail, M.S. Salihatun, M.N.A. Rahman, S. Mahzan, S.S. Ayop, A comparative study of turbulence models on aerodynamics characteristics of a NACA0012 airfoil, Int. J. Integrat. Eng. 10 (1) (2018) 134–137.
[20] N. Pellerin, S. Leclaire, M. Reggio, An implementation of the Spalart-Allmaras turbulence model in a multi-domain Lattice Boltzmann method for solving turbulent airfoil flows, Comput. Math. Appl. 70 (12) (2015) 3001–3018, https://doi.org/10.1016/j.camwa.2015.10.006.
[21] A. Crivellini, V. D'Alessandro, Spalart-Allmaras model apparent transition and RANS simulations of laminar separation bubbles on airfoils, Int. J. Heat Fluid Flow 47 (2014) 70–83, https://doi.org/10.1016/j.ijheatfluidflow.2014.03.002.
[22] M.A. Sayed, H.A. Kandil, A. Shaltot, Aerodynamic analysis of different wind-turbine-blade profiles using finite-volume method, Energy Convers. Manag. 64 (2012) 541–550.
[23] H. Yang, W. Shen, H. Xu, Z. Hong, C. Liu, Prediction of the wind turbine performance by using BEM with airfoil data extracted from CFD, Renew. Energy 70 (2014) 107–115.
[24] M. Ge, H. Zhang, Y. Wu, Y. Li, Effects of leading edge defects on aerodynamic performance of the S809 airfoil, Energy Convers. Manag. 195 (2019) 466–479, https://doi.org/10.1016/j.enconman.2019.05.026.
[25] C. Suvanjumrat, Comparison of turbulence models for flow past NACA0015 airfoil using OpenFOAM, Eng. J. 21 (3) (2017) 207–221, https://doi.org/10.4186/ej.2017.21.3.207.
[26] ANSYS Inc, ANSYS Fluent 15.0 Theory Guide, 2013. Tech. rep., Canonsburg, PA, USA.
[27] M. Özkan, P.J. Thomas, A.J. Cooper, S.J. Garrett, Comparison of the effects of surface roughness and confinement on rotor stator cavity flow, Eng. Appl. Comput. Fluid Mech. 11 (1) (2017) 142–158, https://doi.org/10.1080/19942060.2016.1247297.
[28] M. Hansen, J. Sã,rensen, S. Voutsinas, N. Sã,rensen, H. Madsen, State of the art in wind turbine aerodynamics and aeroelasticity, Prog. Aero. Sci. 42 (4) (2006) 285–330, https://doi.org/10.1016/j.paerosci.2006.10.002.
[29] E. Hoogedoorn, G.B. Jacobs, A. Beyene, Aero-elastic behavior of a flexible blade for wind turbine application: a 2D computational study, Energy 35 (2) (2010) 778–785, https://doi.org/10.1016/j.energy.2009.08.030.
[30] M. Mohamed, Performance investigation of H-rotor Darrieus turbine with new airfoil shapes, Energy 47 (1) (2012) 522–530, https://doi.org/10.1016/j.energy.2012.08.044.
[31] R.K. Singh, M.R. Ahmed, M.A. Zullah, Y.-H. Lee, Design of a low Reynolds number airfoil for small horizontal axis wind turbines, Renew. Energy 42 (2012) 66–76, https://doi.org/10.1016/j.renene.2011.09.014.
[32] L. Daróczy, G. Janiga, K. Petrasch, M. Webner, D. Thévenin, Comparative analysis of turbulence models for the aerodynamic simulation of H-Darrieus rotors, Energy 90 (2015) 680–690, https://doi.org/10.1016/j.energy.2015.07.102.
[33] Y. Wang, S. Shen, G. Li, D. Huang, Z. Zheng, Investigation on aerodynamic performance of vertical axis wind turbine with different series airfoil shapes, Renew. Energy 126 (2018) 801–818, https://doi.org/10.1016/j.renene.2018.02.095.
[34] M.R. Castelli, A. Englaro, E. Benini, The Darrieus wind turbine: proposal for a new performance prediction model based on CFD, Energy 36 (8) (2011) 4919–4934, https://doi.org/10.1016/j.energy.2011.05.036.
[35] I. Abbott, A. Von Doenhoff, Theory of Wing Sections, Including a Summary of Airfoil Data, Courier Corporation, New York, USA, 1959.
[36] T. Burton, N. Jenkins, D. Sharpe, E. Bossanyi, Wind Energy Handbook, second ed., John Wiley & Sons, West Sussex, UK, 1959.
[37] NACA, Airfoil Tools. http://airfoiltools.com/airfoil/details?airfoil=n63415-il. (Accessed 25 July 2019).
[38] M.O.L. Hansen, Aerodynamics of Wind Turbines, second ed., Earthscan Publications Ltd., London, UK, 2008.
[39] A.M. Kuethe, C.Y. Chow, Foundations of Aerodynamics, fifth ed., John Wiley & Sons, New York, USA, 1998.
[40] G.K. Batchelor, An Introduction to Fluid Dynamics, Cambridge University Press, Cambridge, UK, 1967.
[41] N.J. Mulvany, L. Chen, J.Y. Tu, B. Anderson, Steady-state Evaluation of Two-Equation RANS (Reynolds-averaged Navier-Stokes) Turbulence Models for High-Reynolds Number Hydrodynamic Flow Simulations, 2004. Tech. rep., Victoria, Australia.
[42] J.O. Hinze, Turbulence, McGraw-Hill Publishing Co., New York, USA, 1975.
[43] X. Munduate, E. Ferrer, CFD predictions of transition and distributed roughness over a wind turbine airfoil, in: 47th AIAA Aerospace Sciences Meeting Including the New Horizons Forum and Aerospace Exposition, 2009, https://doi.org/10.2514/6.2009-269.
[44] K. Gharali, D.A. Johnson, Numerical modeling of an S809 airfoil under dynamic stall, erosion and high reduced frequencies, Appl. Energy 93 (2012) 45–52, https://doi.org/10.1016/j.apenergy.2011.04.037.
[45] M. Liu, L. Tan, S. Cao, Theoretical model of energy performance prediction and BEP determination for centrifugal pump as turbine, Energy 172 (2019) 712–732, https://doi.org/10.1016/j.energy.2019.01.162.
[46] Y. Liu, L. Tan, Tip clearance on pressure fluctuation intensity and vortex characteristic of a mixed flow pump as turbine at pump mode, Renew. Energy 129 (2018) 606–615, https://doi.org/10.1016/j.renene.2018.06.032.
[47] Y. Hao, L. Tan, Symmetrical and unsymmetrical tip clearances on cavitation performance and radial force of a mixed flow pump as turbine at pump mode, Renew. Energy 127 (2018) 368–376, https://doi.org/10.1016/j.renene.2018.04.072.
[48] H. Salem, A. Diab, Z. Ghoneim, CFD simulation and analysis of performance degradation of wind turbine blades in dusty environments, in: 2013 International Conference on Renewable Energy Research and Applications, ICRERA, 2013, pp. 827–832, https://doi.org/10.1109/ICRERA.2013.6749867.
[49] O. Erkan, M. Ozkan, Investigation of the flow over NACA 63-415 airfoil, BSJ Eng. Sci. 3 (2) (2020) 50–56, https://doi.org/10.34248/bsengineering.643916.
[50] C. Bak, P. Fuglsang, J. Johansen, I. Antoniou, Wind Tunnel Tests of the NACA 63-415 and a Modified NACA 63-415 Airfoil, Tech. Rep. Risø-R-1193, Risø National Laboratory, Roskilde, Denmark, 2000.
[51] P. Fuglsang, C. Bak, Modification of the NACA 63-415 leading edge to avoid double stall, in: Proceedings of the 13th IEA Symposium on the Aerodynamics of Wind Turbines, Stockholm, Sweden, 1999.
[52] I. Yilmaz, O. Cam, M. Tastan, A. Karci, Experimental investigation of aerodynamic performance of different wind turbine airfoils, J. Polytech.-Politeknik Dergisi 19 (4) (2016) 577–584.